OPEN ACCESS

Marine Science ARTICLE

Stoichiometric acclimation of phytoplankton shapes the nitracline

Moge Du,[1,*] Judith Camps-Castellà,[2] Meng Gao,[1] and Keisuke Inomura[1,*]

*Correspondence: moge.du@uri.edu (M.D.); inomura@uri.edu (K.I.)

Received: January 5, 2026; Accepted: June 22, 2026; Published Online: June 29, 2026; https://doi.org/10.59717/j.xinn-geo.2026.100230

GRAPHICAL ABSTRACT

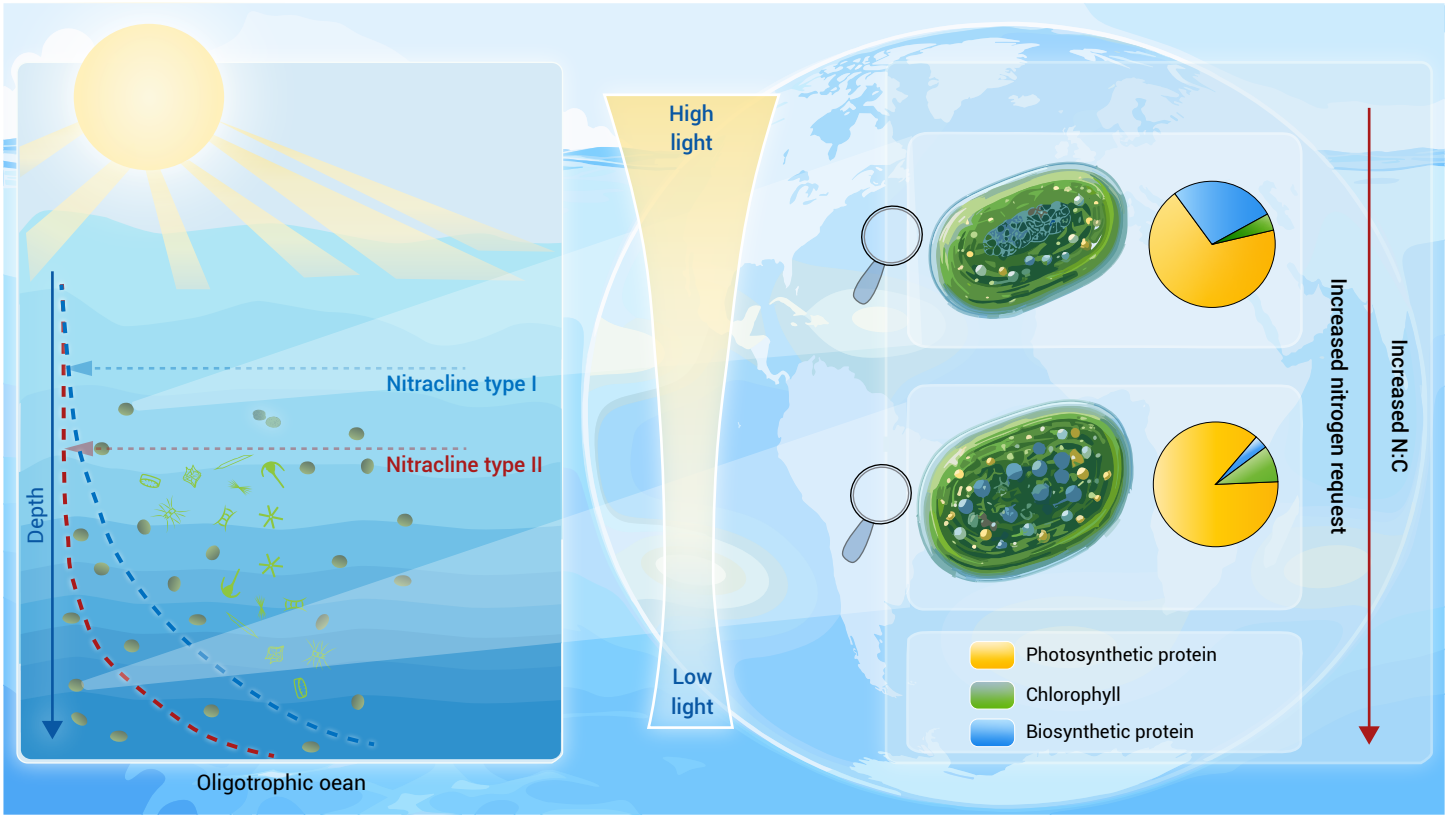

PUBLIC SUMMARY

- A novel water column model bridges the cellular mechanism and systematical vertical nutrient distributions.
- Low-light conditions increase phytoplankton N:C ratio, deepening the nitracline by raising nitrogen demand.
- Higher biological N demand depletes ambient nitrate and reshapes the nitracline beyond physical mixing.

ARTICLE Marine Science

OPEN ACCESS

Stoichiometric acclimation of phytoplankton shapes the nitracline

Moge Du,[1,*] Judith Camps-Castellà,[2] Meng Gao,[1] and Keisuke Inomura[1,*]

[1]Graduate School of Oceanography, University of Rhode Island, Narragansett RI 02882, USA

[2]Departament de Biologia Evolutiva, Ecologia i Ciències Ambientals, Facultat de Biologia, Universitat de Barcelona, Barcelona 08028, Spain

*Correspondence: moge.du@uri.edu (M.D.); inomura@uri.edu (K.I.)

Received: January 5, 2026; Accepted: June 22, 2026; Published Online: June 29, 2026; https://doi.org/10.59717/j.xinn-geo.2026.100230

Citation: Du M., Camps-Castellà J., Gao M., et al. (2026). Stoichiometric acclimation of phytoplankton shapes the nitracline. *The Innovation Geoscience* **4**:100230.

Nitracline is a critical boundary in the ocean, regulating nitrate supply and primary productivity. However, the explicit mechanisms governing its depth in the vast oligotrophic ocean remain a puzzle. Although traditionally regarded as a structure imposed by physical processes, the nitracline may also be modulated by ecological feedback from phytoplankton, which has received far less attention. Here, by combining the mechanistic model of phytoplankton with a water column framework, we identify that the physiological acclimation of phytoplankton plays a central role in deepening the nitracline. Near the bottom of the euphotic zone, light availability becomes scarce. However, phytoplankton can still sustain photosynthesis and growth there by allocating more carbon and nitrogen to photosynthetic molecules. Because these photosynthetic molecules are nitrogen-rich, phytoplankton increases their nitrogen uptake to maintain photosynthetic function, thereby drawing down nitrate and deepening the nitracline. The influence of this physiological acclimation on nitracline depth is demonstrated by comparing simulations with variable versus fixed cellular C:N ratios. The flexiable C:N contributes to the nitracline deepening while the fixed C:N ratio yielded a significantly shallower nitracline. Our study mechanistically connects plankton physiology and the depth profile of marine chemistry, the knowledge essential in predicting future shifts in marine biogeochemical cycling.

INTRODUCTION

Nitrate is an important nutrient for phytoplankton growth in the oligotrophic ocean. In surface waters, nitrate is generally depleted, while in deeper waters it becomes replete. This vertical distribution produces a layer where nitrate concentration increases rapidly with depth, shaping a significant nitrate gradient, known as the nitracline. This gradient regulates the upward nitrate flux into the euphotic zone,[1] thereby fueling the phytoplankton growth and plays a central role in primary production.[2–4]

As a gatekeeper of vertical nutrient transport, nitracline serves as a robust boundary which corresponds to community interaction and biological dynamics. In the stratified ocean, The position of the nitracline marks a distinct transition in ammonium fate, delineating the biological uptake zone from the microbial nitrification layer.[5] Additionally, regional studies in the eastern Indian Ocean demonstrate that shallow nitracline associated with higher upward nitrate supply corresponded to low nitrogen fixation rates.[6] In less-oligotrophic or mesotrophic waters, the subsurface chlorophyll maximum layer shows tight coupling with nitracline.[7] At basin scale, the primary nitrite maxima (PNM) presents significant positive correlation with the nitracline depth, as nitracline depth regulates the competitive interactions between phytoplankton and nitrifiers, thereby controlling the geographic distribution of nitrite.[8] Beyond being a biogeochemical boundary, nitracline is fundamentally linked to the physical structure of the water column. At the Bay of Bengal, the nitracline depth shows a linear correlation with the 26°C isotherm.[4] In the North Pacific ocean, mesoscale eddies shoal the nitracline for weeks to months, stimulating increases in surface chlorophyll.[9] Despite the known importance of nitracline, the factors controlling its depth remain unresolved.

Multiple observations highlight that light plays a key role in controlling the nitracline. In the tropical Atlantic, the nitracline remains relatively constant near the 1% surface light level, even when the 26.0 $kg{\cdot}m^{-3}$ isopycnal varies widely, suggesting that optical rather than density structure governs its depth.[2] In the North Pacific Subtropical Gyre, both surface light and its attenuation within the water column strongly influence nitrate dynamics[10]. In stratified waters, the steepness of the nitracline correlates with the light attenuation coefficient but not with surface irradiance.[11] Observations at the Bermuda Atlantic Time-series Station (BATS) have shown that the nitracline can extend deeper than the 1% isolume, while the nitracline often presents deeper layer where phytoplankton cells have been detected at depths approaching 150 m.[12] However, long-term observations at the Hawaii Ocean Time-series (HOT) station ALOHA show that the nitracline deepens in summer compared to winter, with lower nitrate concentrations, yet consistently remains shallower than the euphotic zone defined by the 1% surface light level.[10] On a global scale, further analyses reveal that the depths of the nitracline and the euphotic zone do not consistently coincide.[13] However, those statistical and empirical knowledge are limited, and the biological mechanism controlling the depth of the nitracline remained unknown.

To address this gap, we investigate how phytoplankton physiology actively reshapes the nitracline by developing a novel water column model that incorporates dynamic cellular physiology. Our model explicitly resolves how phytoplankton adapts to low light by increasing the nitrogen allocation to their photosynthetic apparatus with a macromolecular framework. This stoichiometric acclimation of phytoplankton enhances nitrate uptake and simultaneously sustains their growth, thereby creating a feedback loop. We then compare our model to a traditional NPZD model. This comparison highlights that representing this flexible phytoplankton stoichiometry (driven by photoacclimation and ambient nutrient) is critical for accurately linking cellular nitrogen demand to the nitracline's depth, a linkage essential for predicting biogeochemical responses to environmental change.

MATERIALS AND METHODS

Model structure: Simplified nitrogen ecosystem model (sNECO) and cell flux model (CFM)

For an explicit explanation of the photophysiological effects on nitracline, we developed two water column models with core modules that (1) a simplified nitrogen-based ecosystem model incorporated with nutrient, phytoplankton and detritus (sNECO) and (2) a cell flux model of phytoplankton (CFM). These two models all parameterized the nitrogen dynamics including uptake, nitrification and remineralization. Thus, the biological structure in the water column can be simulated by the nitrogen turnover within various dissolved and particulate pools (Figure 1). *Synechococcus* is set as the simulated functional phytoplankton in models because of the high effective utilization of nitrate compared with other picophytoplankton.

In sNECO model (A), nitrogen is the currency. The growth of phytoplankton is equivalent to the nitrogen uptake rate, which is, all nitrogen uptake by phytoplankton is converted to biomass, and the cellular nitrogen to carbon ratio is fixed following the conventional Redfield ratio (N:C = 16:106). In CFM (B), the nitrogen uptake by phytoplankton is allocated to cell fundamental maintenance and growth, the N:C is varied with the light intensity and ambient substrate concentration. Both simulated phytoplankton in these two models prefer ammonium (NH_4^+) to nitrate (NO_3^-) when uptake N nutrients.

The sNECO is a simplified version of water column model published by Zakem et al.,[14] which takes nitrogen (N) as currency, that is, all nutrients concentration, detritus and phytoplankton biomass are calculated in N content. The carbon and nitrogen cell quota is fixed and can be mutually converted by the conventional Redfield ratio of C:N = 6.625. By contrast, the CFM sets a flexible cellular nitrogen quota for phytoplankton, which is regulated by cell physiology and a fixed cellular carbon quota for reference. Specifically, the cellular N quota varies with the dynamic cellular N uptake, allocation and exudation, which are explicitly implemented by macromolecular allocation associated with photosynthesis, biosynthesis, and maintenance that respond to the ambient nutrient and light availability (Figure 2).

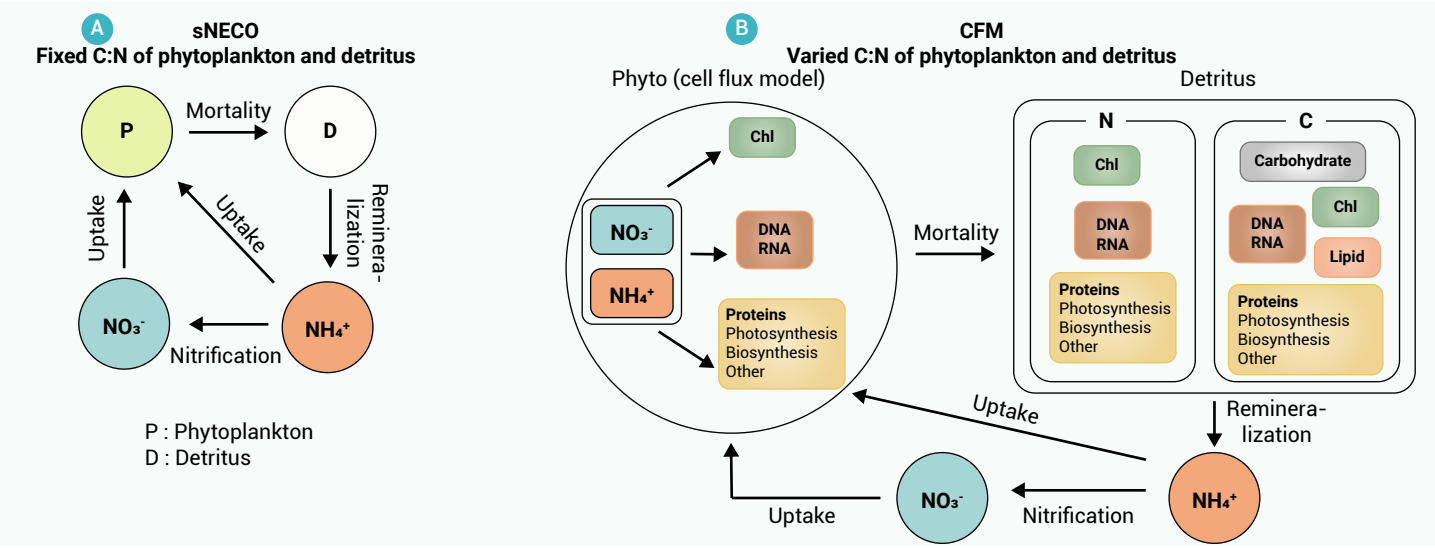

Figure 1. Structures of simplified nitrogen ecosystem model (sNECO) and cell flux model (CFM).

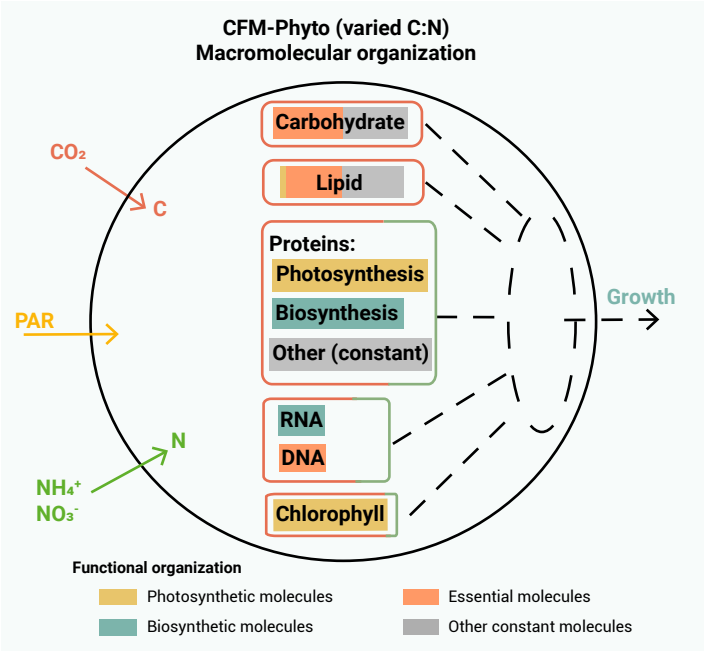

Figure 2. Schematic of macromolecular allocation of cell flux model.

Each molecular with color box represents the allocation of carbon (pink) and nitrogen (green) to their pools. We organized macromolecular into 4 functional groups: photosynthesis, biosynthesis, essential and others. Photosynthetic macromolecular include photosynthetic proteins, chlorophyll, and lipid in the thylakoid membranes. Biosynthetic macromolecular include biosynthetic proteins and RNA. Essential macromolecular include the necessary molecules for cell basic maintenance (such as DNA, a minimum level of proteins) and cell structure (such as lipid in membrane and carbohydrate), the remaining carbon is grouped to others. Molecular with different highlighting background represents their physiological functions. Since we consider cell growth in oligotrophic environment, there are no storage pools of carbon and nitrogen. All elements are utilized for cell growth or/and fundamental maintenance.

Parameterization of biological processes

Mortality. For both sNECO and CFM, we set the quadratic mortality terms (m_{sNECO} and m_{CFM}) balanced with the growth. Note that we do not include explicit losses induced by grazing or viruses in this study. Since the mortality in sNECO is calculated by nitrogen loss while in CFM it is by cell abundance loss, we conduct unit conversion for these two parameter values settings.

The conversion was derived by equating the total nitrogen mortality flux (in mol·N·m^{-3}·day^{-1}) between the models (equation (1)). This flux is defined as $m_{sNECO} \cdot X^2_{sENCO}$ in sNECO (where X_{sNECO} isnitrogen content in mol·N·m^{-3}) and as the nitrogen equivalent of the CFM, $m_{CFM} \cdot X^2_{CFM} \cdot Q_N \cdot 1000$.

The conversion relies on the cellular nitrogen quota (Q_N, in mol·N·cell^{-1}) and the volume conversion factor (1000 L·m^{-3}). Given the state variable relationship $X_{sNECO} = X_{CFM} \cdot Q_N \cdot 1000$, the relationship between the rate parameters simplifies to:

$$m_{sNECO} = \frac{m_{CFM}}{Q_N \times 1000} \quad (1)$$

Considering the steady state when the growth rate is balanced with mortality rate, the theoretical cell abundance would be $\frac{\mu}{m_{CFM}}$. By assuming the *Synechococcus* abundance of ~10^7 cells·L^{-1}, and the growth rate of ~1 day^{-1}, we can estimate the m_{CFM} to be ~ 10^{-7} (cells·L^{-1})$^{-1}$·day^{-1}. The other necessary parameter for estimating the comparable mortality in sNECO is Q_N. This cellular nitrogen content value is set as 4.0 fmol·N·cell^{-1}, which is synthesized from multiple laboratory studies on oceanic *Synechococcus*[15–18] and is in strong agreement with the mean value (3.5 ± 2.8 fmol·N·cell^{-1}) measured from natural populations in the North Atlantic Ocean,[19] making it a robust and representative parameter.

Finally, by substituting m_{CFM} and Q_N in the above formula, we can obtain the mortality in sNECO of 2.5 × 10^4 (mol·N·m^{-3})$^{-1}$·day^{-1}.

Photosynthetic rate

In sNECO, the photosynthetic rate γ (mol·C·(mg·Chl)$^{-1}$·day^{-1}) was computed as a simplified function of photosynthetically active radiation I (μmol·photons·m^{-2}·s^{-1}), the maximum quantum yield of carbon fixation ϕ (mol·C·mol^{-1}·photons), and the absorption of light by phytoplankton a^{chl}_{phy} (m^2·(mg·Chl)$^{-1}$) representing a mean value over all wavelengths,[20] as:

$$\gamma = \phi * a^{chl}_{phy} * I \quad (2)$$

The unit of photosynthetic rate in sNECO is calculated by per chlorophyll weight. The initial slope of this parameterized P-I curve is 1.053 × 10^{-4} mol·C·(mol·C in Chl)$^{-1}$·m^2·μmol^{-1} (Table S1).

In CFM, the photosynthetic rate $\upsilon(I)$ followed the exponential saturation function of irradiance I:

$$\upsilon(I) = v^{max}_I * (1 - e^{-A_i * I}) \quad (3)$$

Where v^{max}_I is the maximum photosynthetic rate per chlorophyll (mol·C·(mol·C in Chl)$^{-1}$·s^{-1}), A_i is the coefficient characterizing the absorption cross-section and turnover time of the photosynthetic unit (μmol^{-1}·m^2·s), I is the photosynthetic active radiation (μmol·quanta·m^{-2}·s^{-1}). The initial slope of

P-I curve of this parametrization is 1.056×10^{-4} mol·C·(mol·C in Chl)$^{-1}$·m^2·μmol^{-1} (Table S1).

Chl:C. The chlorophyll to carbon ratio varied with photoacclimation, which is a response to an imbalance between the rate of light absorption and the energy demands for photosynthesis and biosynthesis.[21] In sNECO, Chl:C (θ, unit: g·Chl·mol^{-1}·C) is constrained by a fixed range ($[\theta_{min}, \theta_{max}]$) and varied with the light and nutrient availability, its calculation follows function at steady state:[21]

$$\theta = \frac{\theta_{max}}{1 + \frac{\Gamma\theta_{max}}{2\mu_{max}\left(\frac{NH_4^+}{NH_4^+ + K_{NH4,P}} + \frac{NO_3^-}{NO_3^- + K_{NO3,P}}\right)}} \tag{4}$$

where μ_{max} is a fixed value of maximum specific uptake rate, and because all the uptake nitrogen is considered as phytoplankton biomass, the uptake rate here is equal to the growth rate. γ is the photosynthetic rate mentioned above. NH_4^+ and NO_3^- are ambient nutrient concentrations. $K_{NH4,P}$ and $K_{NO3,P}$ are the phytoplankton uptake half-saturation constants for NH_4^+ and NO_3^-, respectively.

While in CFM, the Chl:C is calculated based on the carbon allocation to photosynthetic machinery, specifically, the change rate of cellular carbon quota C_{cell} (mol·C·cell^{-1}) is increased by photosynthesis, and reduced division with population growth μ (day^{-1}) and maintenance respiration rate m (day^{-1}):

$$\frac{dC_{cell}}{dt} = v_I Q_C^{Chl} C_{cell} - (1+E) C_{cell}\mu - mC_{cell} \tag{5}$$

where Q_C^{Chl} is cellular chlorophyll to cellular carbon ratio ((mol·C in Chl)·mol^{-1}·C), and v_I is the per chlorophyll rate of photosynthesis as defined in equation (3). E is the respiratory cost of synthesis (moles C respired per mole C synthesized) (see details in Keisuke et al.[22]).

At steady state, $\frac{dC_{cell}}{dt} = 0$, the Q_C^{Chl} can be solved as:

$$Q_C^{Chl} = \frac{1+E}{v_I}\mu + \frac{m}{v_I} \tag{6}$$

This solution anticipates the observed linear relationship between the cellular chlorophyll to carbon ratio ($Q_C^{Chl} = Chl{:}\,C$) and growth rate for any given photon flux, I.

Additionally, in CFM, the maximum cellular chlorophyll is constrained by carbon allocation under low-light conditions. Except for chlorophyll, photosynthetic machinery also includes light-related proteins $Q_C^{Pro-Pho}$ (mol·C in photosynthetic protein per cell) and the thylakoid phospholipids Q_P^{Thy} (mol·C in thylakoid phospholipids per cell). These three components co-vary linearly. In other words, they constitute thylakoid apparatus of which composition remains constant, but its amount per cell is varied with acclimation.

$$Q_C^{Pro-Pho} = A_{pho} Q_C^{Chl} \tag{7}$$

$$Q_P^{Thy} = Y^{P:\,Chl}_{thylakoidPG} Q_C^{Chl} \tag{8}$$

where A_{pho} and $Y^{P:\,Chl}_{thylakoidPG}$ are constants of proportionality.

Under extreme low light conditions, there is no carbon allocated to biosynthesis (growth rate is zero), cellular carbon is only allocated to the necessary parts of DNA (C_{const_dna}), RNA (C_{const_rna}), protein ($C_{const\_protein}$) and the essential components ($C_{essential}$), e.g., the constant components of lipid and carbohydrate, the other carbon (C_{remain}) is allocated to the photosynthetic apparatus that mentioned above. This strategy cuts off cell division for its fundamental maintenance. Since the carbon allocation in chlorophyll is increased with decreased light, the cellular chlorophyll reaches maximum that constrained by the carbon allocation under critical light level:

$$C_{remain} = C_{cell} - C_{const\_dna} - C_{const\_rna} - C_{const\_protein} = C_{photo} + C_{Chl} + C_{thylakoidPG} \tag{9}$$

since $C_{photo}{:}\,C_{Chl}{:}\,C_{thylakoidPG} = Y^{N:\,Chl}_{photo} Y^{C:\,N}_{protein}{:}\,1{:}\,Y^{P:\,Chl}_{thylakoidPG} Y^{C:\,P}_{pg}$, we can obtain the maximum Chl:C under low light in CFM as:

$$C_{Chlmax} = C_{remain} * \frac{1}{Y^{N:\,Chl}_{photo} Y^{C:\,N}_{protein} + 1 + Y^{P:\,Chl}_{thylakoidPG} Y^{C:\,P}_{pg}} \tag{10}$$

and naturally the carbon allocation to photosynthetic protein and the lipid in thylakoid membrane can be obtained:

$$C_{photo} = C_{remain} * \frac{Y^{N:\,Chl}_{photo} Y^{C:\,N}_{protein}}{Y^{N:\,Chl}_{photo} Y^{C:\,N}_{protein} + 1 + Y^{P:\,Chl}_{thylakoidPG} Y^{C:\,P}_{pg}} \tag{11}$$

$$C_{thylakoidPG} = C_{remain} * \frac{Y^{P:\,Chl}_{thylakoidPG} Y^{C:\,P}_{pg}}{Y^{N:\,Chl}_{photo} Y^{C:\,N}_{protein} + 1 + Y^{P:\,Chl}_{thylakoidPG} Y^{C:\,P}_{pg}} \tag{12}$$

Growth rate of phytoplankton. In sNECO, as mentioned above, all the uptake nitrogen counts to the biomass content growth, the uptake rate, as to the population growth rate μ (day^{-1}) of phytoplankton is regulated by nutrients $f(N)$ and light $g(I)$:

$$\mu = \mu_{max} f(N) g(I) \tag{13}$$

where $f(N) = \frac{NH_4^+}{NH_4^+ + K_{NH4,P}} + \frac{NO_3^-}{NO_3^- + K_{NO3,P}}$ and $g(I) = 1 - e^{-\frac{\theta}{\mu_{max} f(N)}}$.

In CFM, the phytoplankton growth rate is calculated based on the carbon and nitrogen allocation. Phosphate (P) is not a limiting factor for cell growth, so whichever macromolecular needs P, it is sufficient for growth and cell survival. Cellular carbon is the sum of all C pools (Figure 2):

$$C_{cell} = C_{pro} + C_{rna} + C_{dna} + C_{chl} + C_{thylakoidPG} + C_{essential} + C_{other} \tag{14}$$

where $C_{thylakoidPG}$ denotes the lipid molecular in thylakoid membrane, and $C_{essential}$ includes the essential non-flexible components of lipid membrane and carbohydrate, the remaining carbon are organized to C_{other}. Take the carbon content in the cells as one equivalent, we have:

$$1 = Q_c^{Pro} + Q_c^{RNA} + Q_c^{DNA} + Q_c^{Chl} + Q_c^{ThylakoidPG} + Q_c^{Essential} + Q_c^{Other} \tag{15}$$

Key assumptions of cell flux model include:

1. Linear relationships between the proteins, RNA and growth rate.[22] Thus, we have:

$$Q_c^{Pro} = Q_c^{Pro-bio} + Q_c^{Pro-pho} + Q_c^{Pro-oth} \tag{16}$$

$$Q_c^{Pro-bio} = A_{bio}\mu \tag{17}$$

$$Q_c^{Pro-pho} = A_{pho} Q_c^{Chl} \tag{18}$$

$$Q_c^{RNA} = Q_P^{RNA} Y^{C:\,P}_{RNA} \tag{19}$$

$$Q_P^{RNA} = A^P_{RNA}\mu Q_c^{Pro} + Q^{RNA}_{P,min} \tag{20}$$

2. Constant macromolecular composition of photosynthetic machinery.

3. Saturating function between irradiance and photosynthetic rate.

Phosphatidylglycerol is the main phosphorus lipid stored in the thylakoid membrane. Because it is structurally integrated with photosynthetic complexes, its contribution to thylakoid phosphorus (Q_P^{Thy}) scales directly with the amount of chlorophyll (Q_c^{Chl}), resulting in a linear relationship between the two:

$$Q_C^{Plip-Thy} = Q_P^{Thy} Y^{C:\,P}_{Plip} \tag{21}$$

$$Q_P^{Thy} = Y^{P:\,Chl}_{thylakoidPG} Q_c^{Chl} \tag{22}$$

Based on the above equations, we have

$$0 = a_C\mu^2 + b_C\mu + c_C \tag{23}$$

where

$$a_C = Y^{C:\,P}_{RNA} A^P_{RNA}\left(A_{pho}\frac{1+E}{\upsilon(I)} + A_{bio}\right) \tag{24}$$

$$b_C = \left(1 + A_{pho} + Y^{C:\,P}_{Plip} Y^{P:\,Chl}_{thylakoidPG}\right)\frac{1+E}{\upsilon(I)} + A_{bio} + Y^{C:\,P}_{RNA} A^{RNA}_P\left(A_{pho}\frac{m}{\upsilon(I)} + Q_c^{Pro-oth}\right) \tag{25}$$

$$c_C = \left(1 + A_{pho} + Y^{C:P}_{Plip} Y^{P:Chl}_{thylakoidPG}\right) \frac{m}{U(I)} + Q^{Essential}_c + Q^{Other}_c + Y^{C:P}_{RNA} Q^{RNA}_{P,min} - 1 \quad (26)$$

This solution for μ is the growth rate based on carbon allocation, in other words, under C limitation but N is sufficient.

As for the N limitation, we consider the cellular nitrogen Q_N change rate varies with growth μ and nitrogen uptake V_N:

$$\frac{dQ_N}{dt} = V_N - \mu Q_N \quad (27)$$

At steady state, $\frac{dQ_N}{dt} = 0$, then we have $V_N = \mu Q_N$

The nitrogen uptake is limited by diffusion under N limitation; thus the uptake rate is proportional to the ambient nutrient concentration:

$$V_N = a_{NH4} NH_4^+ + a_{NO3} NO_3^- \quad (28)$$

where a_{NH4} and a_{NO3} is the affinity for NH_4^+ and NO_3^-, respectively.

The cellular nitrogen is allocated to macromolecular pools include protein Q_N^{Pro}, RNA Q_N^{RNA}, DNA Q_N^{DNA}, chlorophyll Q_N^{Chl}, thus we have:

$$Q_N = Q_N^{Pro} + Q_N^{RNA} + Q_N^{DNA} + Q_N^{Chl} \quad (29)$$

By rearrangement, we have:

$$0 = a_N \mu^3 + b_N \mu^2 + c_N \mu + d_N \quad (30)$$

where

$$a_N = Y^{N:P}_{RNA} A^P_{RNA} \left(A_{pho} \frac{1+E}{U(I)} + A_{bio}\right) \quad (31)$$

$$b_N = Y^{N:C}_{Chl} \frac{1+E}{U(I)} + Y^{N:C}_{Pro} \left(A_{bio} + A_{pho} \frac{1+E}{U(I)}\right) + Y^{N:P}_{RNA} A^P_{RNA} \left(A_{pho} \frac{m}{U(I)} + Q^{Pro-oth}_c\right) \quad (32)$$

$$c_N = Y^{N:C}_{Chl} \frac{m}{U(I)} + Y^{N:C}_{Pro} \left(Q^{Pro-oth}_c + A_{pho} \frac{m}{U(I)}\right) + Y^{N:P}_{RNA} Q^{RNA}_{P,min} + Y^{N:C}_{DNA} Q^{DNA}_c \quad (33)$$

$$d_N = -V_N \quad (34)$$

This solution describes the growth rate under nitrogen limitation.

Based on equation (27), the theoretical cellular nitrogen content (Q_N) during each computational step can be calculated using the Euler method. According to the growth status of the cell, the actual nitrogen requirement for biosynthesis and maintenance, denoted as $N_{essential}$, can be determined by the sum of all nitrogen content in each macromolecular ($N_{protein}$+N_{RNA}+N_{DNA}+N_{Chl}). By comparing the theoretically cellular nitrogen after uptake with $N_{essential}$, we can assess the cellular nitrogen balance. When the theoretical nitrogen content is lower than the required amount, all uptake nitrogen is allocated to growth and maintenance. Conversely, when the theoretical nitrogen content exceeds the cellular demand, the excess nitrogen (N_{excess}) is excreted. The excretion flux (V_{exc}) is then used to adjust the theoretical uptake rate (V_N), and the actual nitrogen uptake rate (V_{N_adj}) is obtained by subtracting the excretion rate from the theoretical absorption rate. The equations for excess nitrogen excretion and adjusted uptake rate are as follows:

$$N_{excess} = Q_N - N_{essential} \quad (35)$$

$$V_{exc} = \frac{N_{excess}}{\tau} \quad (36)$$

$$V_{N\_adj} = V_N - V_{exc} \quad (37)$$

where τ is the timescale for the excretion of excess nitrogen.[23]

Nutrient affinity. In sNECO, the nutrient uptake rate follows the Michaelis-Menten equation,

$$V_{NH4} = \mu_{max} \frac{NH_4^+}{NH_4^+ + K_{NH4,P}} P \quad (38)$$

$$V_{NO3} = \mu_{max} \frac{NO_3^-}{NO_3^- + K_{NO3,P}} P \quad (39)$$

where μ_{max} is the maximum growth rate (day^{-1}), which is the equivalent of specific maximum uptake rate. $K_{NH4,P}$ and $K_{NO3,P}$ is the half-saturation constant (K) for NH_4^+ and NO_3^-, respectively. P is the phytoplankton biomass in nitrogen content. Thus, the specific affinity is $\frac{\mu_{max}}{K}$ when ambient nutrient (S) at low concentration, $S \ll K$, which is reasonable in the context of oligotrophic environment. This specific affinity represents the ability of phytoplankton to consume resources per unit biomass.

In CFM, the growth rate is an unknown that needs to be solved, the uptake rate is as follows:

$$V_{NH4} = a_{NH4} \cdot NH_4^+ \quad (40)$$

$$V_{NO3} = a_{NO3} \cdot NO_3^- \quad (41)$$

where a is the cellular affinity for the substrate, in unit of mol N·cell^{-1}·s^{-1} (μmol·N·L^{-1})$^{-1}$. Thus, for the comparability of the simulated results, we set the affinity values in CFM as the specific affinity in sNECO multiple cell nitrogen quota, thus, the values are 4.6296 × 10^{-19} mol·N·cell^{-1}·s^{-1}·(μmol·N·L^{-1})$^{-1}$ and 2.3148 × 10^{-19} mol·N·cell^{-1}·s^{-1} (μmol·N·L^{-1})$^{-1}$ for NH_4^+ and NO_3^- uptake, respectively.

Ammonium regeneration and PON remineralization. In CFM, nitrogen regeneration is the sum of degradation of N-containing detrital components:

$$= \sum_{i=protein,chl,dna,rna}^{i} (d_r * D_{Ci} * D_{Ctotal} * Y_i^{N:C})$$

In CFM, the detritus remineralization follows quadratic terms relating to total detritus concentration and macromolecules:

$$\sum_{i=chl,RNA,DNA,Protein} d_r * D_{Ci} * D_{Ctotal} * Y_i^{N:C}$$

Where d_r defined as degradation rate ((nmol·C·L^{-1})$^{-1}$·day^{-1}), D_{Ci} is the concentration of detrital molecules in carbon contents (nmol·C·L^{-1}), D_{Ctotal} is the total detritus concentration in carbon content (nmol·C·L^{-1}), $Y_i^{N:C}$ is the nitrogen to carbon ration of corresponding macromolecules. This remineralization rate is equal to the ammonium regeneration rate. In this model, we set a fixed degradation rate of 0.016 (nmol·C·L^{-1})$^{-1}$·day^{-1}.

In sNECO, the remineralization, equivalent to the ammonium regeneration, is a simplified quadratic term which is constrained by the organic matter concentration:

$$V_{rem} * PON^2$$

where V_{rem} is a constant degradation rate ((mol·N·m^{-3})$^{-1}$·day^{-1}). Assuming the general organic detritus composition is $C_5H_7O_2N$ which has C:N of 5:1, for comparison with CFM, we set the equivalent V_{rem} as 8.0 × 10^4 (mol·N·m^{-3})$^{-1}$·day^{-1}.

Nitrification. Basically, nitrification in CFM and NECO are both following the Michaelis-Menten equation:

$$V_{nitrification} = nitrif_{max} * \frac{NH_4^+}{NH_4^+ + K_{NH4}(1 + exp(1.4 \cdot ln(Iz) + 0.39))},$$

By adding the light constrain on the half-saturation constant, this equation captures the inhibitory effect of light on the ammonium oxidation process, resulting in increased nitrification within the lower euphotic zone.

Initial conditions

We set the same initial conditions for sNECO and CFM models, including the nutrient concentrations (NH_4^+ and NO_3^-), cell abundance and the consistent physical conditions, surface light intensity, light attenuation coefficient and diffusion coefficient (Figure S1). sNECO applied the same abundance profile as shown in Figure S1 but converted to the unit of nitrogen concentration by the cellular nitrogen quota. As for the detritus, i.e. particulate organic matter, is set to be zero through the water column at the initial state.

RESULTS

The vertical distribution of nitrate

We first quantified the vertical distribution of nitrate in the cell flux model

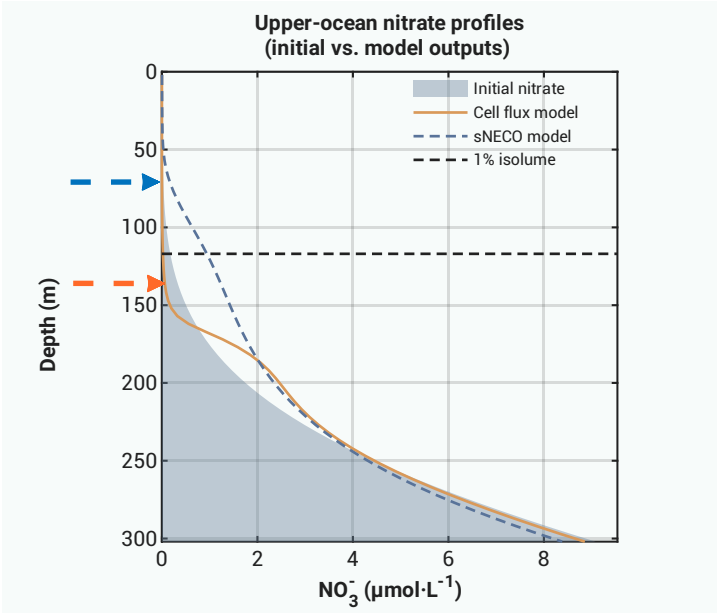

Figure 3. Vertical distribution of simulated nitrate.

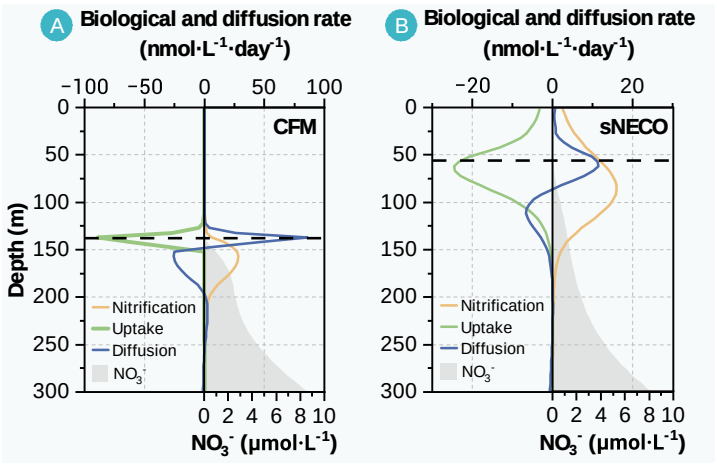

Figure 4. Vertical profiles of nitrate dynamics simulated by (A) CFM and (B) sNECO.

and compared it with the simplified nitrogen ecosystem model. The nitracline delineates the depth at which nitrate increases rapidly and thus provides a compact description of the vertical nitrate structure. Here, we identified the top of the nitracline as the shallowest depth where the vertical nitrate gradient exceeds 2 nmol·kg^{-1}·m^{-1}.[10] For the observations, combined nitrate and nitrite profiles were interpolated to 5-m depth intervals using cubic spline interpolation. Model-derived nitrate profiles have a native 5-m resolution, and we applied the same threshold directly to the simulated profiles to ensure a consistent nitracline definition across datasets.

Our results show that both models reproduce the typical structure of near-surface depletion and a rapid subsurface increase, but they diverge in the vertical position of the nitracline (Figure 3). Using the common criterion, the CFM places the nitracline top at ~138 m, whereas sNECO yields a much shallower value of ~56 m (Figure 3). Below 200 m, the two profiles converge toward similar concentrations. When compared with the light level of 1% isolume, the nitracline in the cell-flux simulation lies below it, while the sNECO nitracline occurs above it. This depth contrast is robust to the choice of gradient threshold. Varying the criterion from 0.001 to 0.003 μmol·L^{-1}·m^{-1} shifts the CFM nitracline top only from ~132 m to ~138 m (Δ ≈ 6 m) and the sNECO value from ~47 m to ~57 m (Δ ≈ 10 m), without altering their relative ordering. These metrics establish a clear structural difference in the simulated vertical nitrate fields: the CFM predicts a deeper nitracline, implying stronger biological regulation and sustained nitrate consumption within the lower euphotic zone, while the sNECO model emphasizes weaker nitrate consumption near the surface, reflecting stronger physical control. Overall, the figure highlights contrasting representations of upper-ocean nitrogen cycling between the two modeling frameworks.

The shading area shows the initial condition, the orange solid and blue dashed lines show the simulated NO_3^- concentration profiles of sNECO and CFM model, respectively. The dashed orange and blue arrows show the depth of the top of the nitracline. The black dashed line shows the 1% surface photosynthetically active radiation isolumes.

In observations, the nitracline-top depth was 89.1±30.2 m (median value is 94.9 m) at HOT and 72.0±30.3 m (median value is 73.6 m) at BATS (Figure S3). Despite both simulations representing phytoplankton that consume nitrate, the two models differ systematically from the observed vertical structure (Figure S5). Relative to the observed median nitracline-top depth, sNECO underestimates the depth at both sites, with a negative bias of 39 m at HOT and a bias of 18 m at BATS, placing the onset of nitrate accumulation too close to the surface. In contrast, the cell-flux model (CFM) overestimates the depth, with a nitracline top of positive bias 43 m at HOT and bias 64 m at BATS. Thus, the observed nitracline lies between the two simulations at both sites: sNECO is systematically too shallow, whereas CFM is systematically deep. This bracketing pattern is robust to the gradient threshold (0.001-0.003 μmol·L^{-1}·m^{-1}). Taking together, these results indicate that the sNECO framework does not capture the observed deep placement of the nitracline, while the CFM, though biased deep, reproduces the tendency toward a deeper nitracline that is more realistic compared with the observation in oligotrophic ocean.

The vertical profiles of nitrate uptake and nitrification

Our simulated results contrast the depth structure of nitrate uptake and nitrification between the two models. In CFM, nitrate uptake exhibits a subsurface maximum coinciding with the nitracline (Figure 4A). Uptake remains appreciable to nearly 150 m before declining. Those nitrate consumption are mainly supported by vertical diffusion within the lower euphotic zone rather than the in-situ nitrification. Similarly, in sNECO, uptake is concentrated well near nitracline, peaking in the upper 50~80 m and declining gradually down to 150 m. However, the nitracline in sNECO is quite shallower than that in CFM, and the nitrate consumption in sNECO is contributed by the comparable source from in-situ nitrification and vertical diffusion (Figure 4B). Thus, the depth of nitrate consumption is systematically deeper in CFM than in sNECO.

Nitrification in CFM features a pronounced subsurface maximum around 160 m, which is deeper than the uptake maximum (Figure 4A), forming a clear separation between biological consumption and regeneration layers. Within the layer shallower than nitracline, the nitrification is vanishingly small but sustains the upward diffusion in deeper layer dominantly. By contrast, nitrification in sNECO presents significant rates within the layer above the nitracline and contributes substantially to the nitrate supply supporting uptake throughout the water column, although its peak also lies deeper than the uptake maximum layer (Figure 4B). Overall, the CFM exhibits a clear vertical decoupling between nitrate consumption and regeneration. This spatial separation drives a deeper nitracline, as the diffusive supply must originate from greater depths to offset upper-ocean uptake. In contrast, the sNECO model co-locates these processes within the upper water column, sustaining a shallower nitracline through immediate local recycling.

The negative values represent the sink terms of nitrate, while the positive values represent the source terms. The dashed line in the two panels shows the top of the nitracline.

Observed nitrification rates in the open ocean generally show a lowest value near the surface ocean, while present subsurface maximum in the deeper layer (Figure S4), spanning about 30 nM·day^{-1} from the surface to 200 m across multiple regions. This unimodal pattern is generally attributed to the light inhibition on nitrifiers[24–26] and the excluding competition by phytoplankton uptake.[5,14,27] The two models capture this range but differ in vertical position of the maximum. The CFM shows a relative consistency with observed nitrification, presents very low rates within the shallow 50 m and has a pronounced subsurface maximum near 160 m (about 30 nM·day^{-1}) (Figure S4). By contrast, sNECO misses the higher nitrification in deeper layer and exhibits elevated rates through the euphotic zone with a peak around 70 m (about 16 nM·day^{-1}) (Figure S4), suggesting a quite different nitrogen cycling

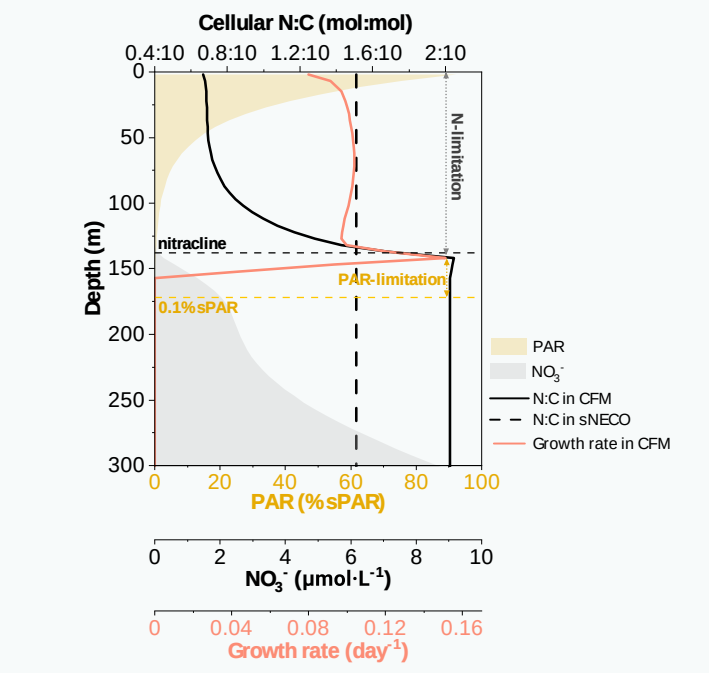

Figure 5. Vertical distribution of cellular nitrogen to carbon ratio and phytoplankton growth rate.

structure with CFM although the two models have the same parameterization scheme except for phytoplankton.

Stoichiometry of simulated phytoplankton

Instead of traditional models with fixed stoichiometry, our model results reveal a pronounced dynamic plasticity in phytoplankton N:C stoichiometry across the water column. In CFM, N:C increases steadily with depth across the euphotic zone, from relatively low values near the surface to a maximum around the nitracline associated with the maximum growth rate (Figure 5). This stoichiometric increase is not stochastic, rather, it is the direct expression of a key physiological trade-off resolved by the cell flux model. The N:C reaches its peak at the intersection of the two regimes, nitrogen limitation and light limitation. To sustain growth under shifting limitation conditions, the model shows that phytoplankton must photoacclimate by synthesizing nitrogen-rich photosynthetic machinery, which is consistent with the extensive laboratory researches.[28–32] It is this physiological plasticity that, by elevating the cellular N:C quota, simultaneously sustains the maximum growth rate at this depth, which is a vital biological process that fixed-stoichiometry models cannot capture.

The dashed and solid lines denote the N:C in sNECO and CFM, respectively. The ecosystem currency in sNECO is nitrogen and it has no explicit stoichiometry for nitrogen and carbon, thus the canonical Redfield ratio (N:C=16:106) is considered as a reference. The yellow and grey shading area denote the percentage of surface photosynthetic radiation and nitrate, respectively. The solid pink line represents the simulated cellular growth rate.

Consequently, this light-driven physiological flexibility generates decisive biogeochemical feedback on the nitrate profile. The model clearly demonstrates that this capacity to sustain maximum growth with elevated N:C within the lower euphotic zone allows phytoplankton to consume the nitrate. This enhanced, *in-situ* biological uptake constitutes the primary nitrate sink for the water column (Figure 4). In doing so, the phytoplankton community actively "sculpts" the morphology of the nitracline itself, fundamentally shaping the depth of its upper boundary and the steepness of its gradient. This finding highlights that neglecting the variability in phytoplankton stoichiometry severely underestimates the biological control on marine nitrate vertical structure.

DISCUSSION

The optical effect on nitracline

The regulation of light availability on the nitracline depth is important in marine biogeochemistry, yet field observations present a complex and often contradictory pattern. In some highly productive regions, such as coastal upwelling systems, a tight, non-linear coupling between water clarity (e.g., Secchi depth) and the nitracline has been reported.[33] This suggests a direct control where light penetration dictates the depth of nutrient utilization. However, this straightforward coupling appears to be an exception rather than the rule at the global scale. A recent, comprehensive analysis of BGC-Argo data by Xing et al.[7] revealed "contrasting relationships" across different oceanographic regimes. They found that while the euphotic zone depth and the nitracline are indeed coupled in some basins, they remain clearly decoupled in others. Critically, Xing et al.[7] attributed this large-scale regional variability to biological mediation, proposing that the coupling is fundamentally determined by the prevailing limitation status (i.e., light- vs. nutrient-limited) of the resident phytoplankton community. This finding strongly indicates that simple statistical or empirical linkages are insufficient to capture the underlying mechanism. Our compiled data at the HOT station (Figure S6), which similarly shows a persistent decoupling between the top of the nitracline and specific isolumes, reinforces this highlight. These contrasting findings collectively establish that light is not a static regulator. Instead, its influence on the nitracline is dynamically mediated by the physiological responses of phytoplankton, which cannot be captured by statistical analyses alone. This establishes the context for the cell flux model, which links the cellular process to the ambient environment to disentangle this complexity.

Our work, by resolving the ecophysiology of *Synechococcus*, provides a direct mechanistical bridge for the N-cost photoacclimation of phytoplankton and ambient nitrate availability. *Synechococcus* allocate a dominant fraction of its cellular nitrogen to building N-rich photosynthetic proteins to maintain light-harvesting (Figure 6), which is consistent with previous research, as PAR attenuates toward the base of the euphotic zone, phytoplankton must photoacclimate, synthesizing extensive photosynthetic machinery that need higher nitrogen allocation (e.g., Photosystems, Rubisco) to maintain light harvesting, a physiological necessity that is fundamentally nitrogen-costly.[22,23] Thus, this general rule is aligned with the field observation showing that particulate N:C gradients are driven by shifts in the relative abundance of N-rich protein versus C-rich carbohydrates and lipids.[34] Moreover, this internal reallocation, in turn, contribute to a stronger and deeper increase in the Chl:C ratios (Figure 7) predicted by CFM and sNECO, consistent with Chl:C being a widely used index for photoacclimation.[31,35,36]

Our cell flux model further reveals the high plasticity of phytoplankton stoichiometry. Mechanistically, total cellular N:C ratio and Chl:N ratio are coupled and must rise concurrently. The N-rich photosynthetic proteins required to increase the Chl:C (the acclimation) driving the increase of the cellular total N-quota (the biogeochemical cost). Field observations provide robust support for this fundamental assumption. Data from Lomas et al.[37] (Figure S5) confirms that *Synechococcus* N:C ratios are not fixed, spanning a wide range (from < 0.8 to > 1.6) that conventional fixed-ratio models (like sNECO) fail to capture. However, we note that those field data do not show the clear and systematic vertical trend predicted by our model. This divergence is expected. Our 1D model intentionally isolates the physiological response to vertical light and nutrient gradients. In contrast, the *in-situ* data reflects a complex interplay of physics (e.g., advection, eddy), regional differences in trace nutrient limitations (e.g., iron), and diverse community structures, all of which can hide the underlying physiological drivers. Therefore, rather than invalidating the model, the observations highlight *why* such process-based models are essential. Such models allow us to disentangle the 'clean' physiological mechanism (which we identified) from the 'noisy' environmental matrix in which it operates, providing a crucial baseline for understanding *why* stoichiometry varies in the real ocean.

This study also provides a significant extension to the theoretical framework of Armstrong[28] where they theorized an optimal N-allocation trade-off between abstract "light-system" and "dark-system" components, our study provides the explicit, macromolecular machinery for this trade-off: we show (Figure 6) that the "light-system" N-cost is the allocation to photosynthetic proteins, while the "dark-system" cost is the N allocated to biosynthetic proteins. More importantly, our work is the first to quantify the external biogeochemical feedback, demonstrating that this cellular, *Synechococcus*-driven N-demand is the mechanism that actively shapes the nitracline itself.

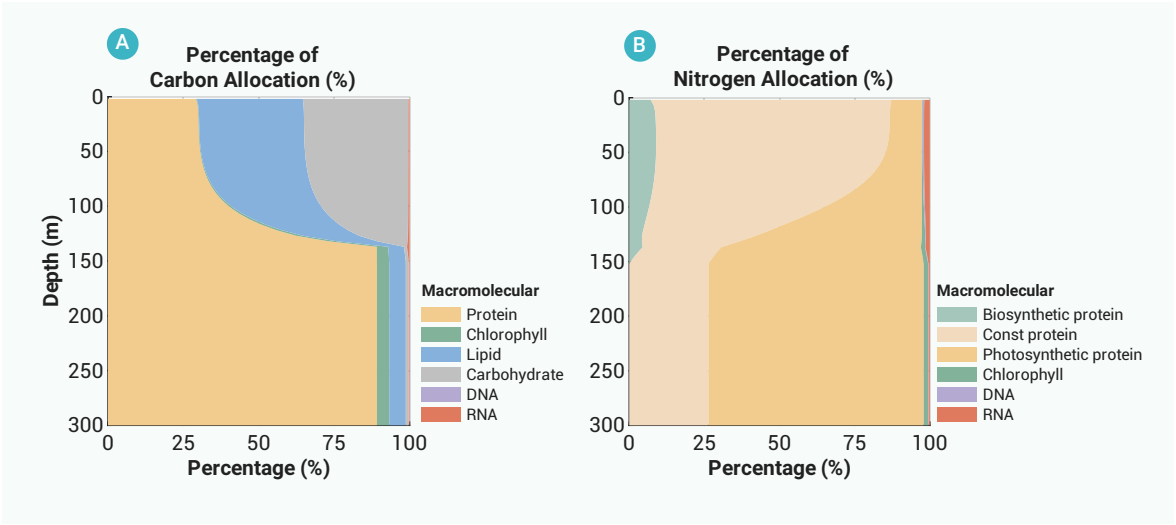

Figure 6. Cellular macromolecular allocation in vertical scale (A) carbon allocation among macromolecular pools and (B) nitrogen allocation among protein functional classes and other macromolecular, shown as stacked - area percentages of the total cellular C or N, respectively.

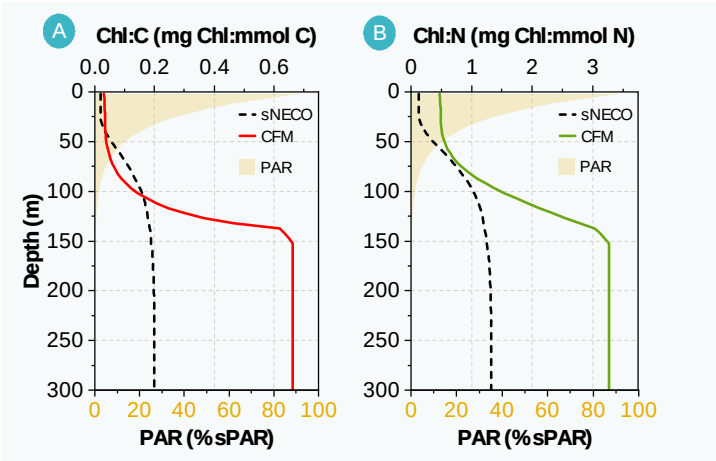

Figure 7. Depth profiles of Chl:C (A) and Chl: N (B) overlaid with PAR (as % of surface) Shaded areas indicate the PAR distribution The CFM (solid) exhibits sustained increases in Chl:C and Chl:N into the lower euphotic zone, whereas sNECO (dashed) shows weaker, shallower responses.

The Chl:C and Chl:N distribution pattern along PAR structure revealed by our results also suggests testable predictions. (i) Across seasons or regions where optical attenuation increases (e.g. larger k), the depth of enhanced Chl:C (or Chl:N) should shoal, and so should the nitracline if physical supply is unchanged. (ii) At a given site, interannual anomalies that shift the depth of the Chl:C (or Chl:N) inflection should covary with the nitracline steepness and the 0.5-1 μM isopleth depths. (iii) Profiles with high Chl:N at 10%-20% surface PAR should exhibit larger nitrate uptake just below the euphotic base and a deeper nitracline relative to profiles lacking this allocation signal. These predictions provide a mechanistic bridge between optical structure and nitracline dynamics that can be evaluated with co-located Chl:C (or Chl:N), PAR, and nitrate profiles from time-series stations and BGC-Argo.

Physical forcing as the envelope for biological control

Our model results reveal that, under identical physical mixing conditions, the stoichiometric acclimation of phytoplankton actively drives the nitracline to a deeper depth compared with the fixed-ratio framework (Figure 3). This shows physics provides the context, while physiology can reshape the ambient nitrate when stratification is stable. Mesoscale eddies act advectively and can shoal isopycnals. Observations in the western North Pacific show that a cyclonic eddy shoaled the 0.1 μM nitracline from about 139 m at the periphery to about 102 m at the core.[12] This kind of uplift compresses the space for a persistent low-light, N-replete niche and moves the system toward a shallower, supply-controlled state that resembles the sNECO outcome. Vertical turbulent mixing acts diffusively. Strong stratification can suppress diapycnal exchange across the nitracline and limit shoaling, which preserves the sharp gradient needed for the CFM mechanism to operate.[1] Breaking internal tides can intensify diapycnal mixing. In the Luzon Strait, microstructure measurements document high vertical diffusivities and a displaced upper nitracline interface that can reach roughly 100–125 m or deeper, together with the presence of oligotrophic Kuroshio water.[38,39] These processes set the physical constraints that either facilitate or suppresses the biological shaping effect. This leads to a regime view that connects back to our simulations. Under intensely mixed, deep mixed-layer conditions, the system is physics-dominated, and phytoplankton residence time in the low-light zone is short, so the nitracline is eroded and the CFM signature weakens,[40] Under strongly stratified, subtropical-like conditions the opposite holds. Stratification limits diapycnal flux from below and maintains a stable, low-light, nitrogen-replete niche. Cells then execute an N-costly, high-N:C acclimation that we resolved (Figure 6). Along the physical processes spectrum, those temporal decoupled physical-biological effects contribute to a weak consistency of nitracline with mixed layer depth in oligotrophic ocean (Figures S6-S7).

To characterize the spatial and temporal variability of nitracline depth, we analyzed vertical nitrate concentration profiles from latitudinal transects spanning 30°N–35°N in the GLODAPv2.2023 database. Despite the well-documented meridional trend of increasing surface ocean nitrate concentration with latitude, our results demonstrate that the temporal variability of nitracline depth at fixed locations (Eulerian observations) is comparable in magnitude to the spatial variability observed across latitude, even in oligotrophic subtropical regions (Figure S8). This comparability suggests short-timescale vertical physical processes, such as internal wave breaking, mixed layer deepening events, and mesoscale/submesoscale circulation features, episodically inject nitrate-enriched deep water into the euphotic zone at rates that exceed the biological response timescale. Given typical phytoplankton nitrate uptake rates ranging from tens to hundreds of nanomoles per liter per day, the complete biological assimilation of micromolar-level nitrate injected from depth requires several weeks. When this biological consumption timescale coincides with or exceeds the recurrence interval of physical mixing events, phytoplankton communities cannot fully deplete the replenished nutrient pool before subsequent physical perturbations occur. Consequently, nitracline depth exhibits sustained temporal variability until the persisting stratification (weeks to months) allows biological processes to dominate over physical forcing, thereby stabilizing the vertical nitrate distribution.

Observation along the North Pacific transect by the community shift also clearly illustrated that this phytoplankton-driven physiological control is not dominant in all regimes (Figure S9). As latitude increases, the system transitions from a stratified, *Prochlorococcus*-dominated regime to a more physically dynamic, nutrient-rich environment. This increased physical nutrient

supply forces a shallower nitracline and, in turn, favors the growth of nitrate-consumers like *Synechococcus* and *Picoeukaryotes*. In this high-latitude, high-biomass regime, the nitracline depth is no longer set by the N-costly physiology of individual cells but is driven by the physical supply from below. Furthermore, as total biomass increases, phytoplankton self-shading likely compresses the euphotic zone, further decoupling the nitracline depth from the specific acclimation strategies we have modeled. Our mechanism is therefore most critical in the vast, stable, oligotrophic gyres where physical processes are retarded, allowing this instant biological feedback to become the dominant sculpting force.

Ultimately, these findings demonstrate that the nitracline is not a static, physically-only defined boundary. Instead, it is a dynamic interface shaped by the competition between physical supply (mixing, eddies) and biological control. In the stratified oligotrophic gyres, our model shows that the N-costly physiology of phytoplankton could be a dominant force, actively depressing the nitracline. This physiological control is likely complemented by the behavioral control proposed by Wirtz & Smith,[41] where active vertical migration by phytoplankton (including *Synechococcus*) creates a "biological nutrient pump".

CONCLUSION

Our study provides a novel, mechanistic explanation for what controls nitracline depth in the oligotrophic ocean. We demonstrate that the nitracline is not only a passive physical boundary but also is actively shaped by biological feedback from phytoplankton ecophysiology. By comparing a traditional fixed-stoichiometry model (sNECO) with a Cell Flux Model (CFM) based on macromolecular allocation, we show that the N-costly strategy of photoacclimation is the critical, missing mechanism. In the low-light, high-nitrate environment of the nitracline, *Synechococcus* allocate a dominant fraction of its cellular nitrogen to N-rich photosynthetic proteins. This physiological necessity drives the cellular N:C ratio to its peak and sustains a high biological nitrate demand at depths where traditional models assume biology has failed. This process actively draws down nitrate far below the 1% isolume, mechanistically explaining the deep nitracline observed in stable, oligotrophic gyres.

This finding address a limitation in traditional Geider-style models, which, as noted by Armstrong,[28] assume that maximum N:C ratios only occur at maximum growth rates. In contrast, our work demonstrate that the N:C peak occurs in the light-limited, low-growth environment near the nitracline, a phenomenon our CFM framework captures. This physiological mechanism provides a biological pathway to sustain production and shape nutrient fields in environments where physical diffusion alone is insufficient. Therefore, to accurately predict nitracline depth and export production, future biogeochemical models must move beyond simple community level response of plankton to environment and incorporate this physiological acclimation of cells, linking the cellular adjustment to the ambient environment.

REFERENCES

1. Du C., Liu Z., Kao S., et al. (2017). Diapycnal fluxes of nutrients in an oligotrophic oceanic regime: The South China Sea. *Geophys. Res. Lett.* **44**:11510–11518. DOI:10.1002/2017GL074921
2. Bahamón N., Velásquez Z. and Cruzado A. (2003). Chlorophyll a and nitrogen flux in the tropical North Atlantic Ocean. *Deep Sea Res. Part I Oceanogr. Res. Pap.* **50**:1189–1203. DOI:10.1016/S0967-0637(03)00145-6
3. Mouriño-Carballido B., Otero Ferrer J.L., Fernández Castro B., et al. (2021). Magnitude of nitrate turbulent diffusion in contrasting marine environments. *Sci. Rep.* **11**:18804. DOI:10.1038/s41598-021-97731-4
4. Sridevi B., Ashitha M.K., Sarma V.V.S.S., et al. (2024). A new climatology of depth of nitracline in the Bay of Bengal for improving model simulations. *J. Geophys. Res. Biogeosci.* **129**:e2024JG008211. DOI:10.1029/2024JG008211
5. Wan X.S., Sheng H.-X., Dai M., et al. (2018). Ambient nitrate switches the ammonium consumption pathway in the euphotic ocean. *Nat. Commun.* **9**:915. DOI:10.1038/s41467-018-03363-0
6. Sato T., Shiozaki T., Hashihama F., et al. (2022). Low nitrogen fixation related to shallow nitracline across the Eastern Indian Ocean. *J. Geophys. Res. Biogeosci.* **127**:e2022JG007104. DOI:10.1029/2022JG007104
7. Xing X., Xiu P., Laws E.A., et al. (2023). Light - driven and nutrient - driven displacements of subsurface chlorophyll maximum depth in subtropical gyres. *Geophys. Res. Lett.* **50**:e2023GL104510. DOI:10.1029/2023GL104510
8. Wan X.S., Sheng H., Dai M., et al. (2021). Phytoplankton - nitrifier interactions control the geographic distribution of nitrite in the upper ocean. *Global Biogeochem. Cycles* **35**:e2021GB007072. DOI:10.1029/2021GB007072
9. Wilson C. (2021). Evidence of episodic nitrate injections in the oligotrophic North Pacific associated with surface chlorophyll blooms. *J. Geophys. Res. Oceans* **126**:e2021JC017169. DOI:10.1029/2021JC017169
10. Letelier R.M., Karl D.M., Abbott M.R., et al. (2004). Light driven seasonal patterns of chlorophyll and nitrate in the lower euphotic zone of the North Pacific Subtropical Gyre. *Limnol. Oceanogr.* **49**:508–519. DOI:10.4319/lo.2004.49.2.0508
11. Gong X., Jiang W., Wang L., et al. (2017). Analytical solution of the nitracline with the evolution of subsurface chlorophyll maximum in stratified water columns. *Biogeosciences* **14**:2371–2386. DOI:10.5194/bg-14-2371-2017
12. Fawcett S.E., Ward B.B., Lomas M.W., et al. (2015). Vertical decoupling of nitrate assimilation and nitrification in the Sargasso Sea. *Deep Sea Res. Part I Oceanogr. Res. Pap.* **103**:64–72. DOI:10.1016/j.dsr.2015.05.004
13. Cornec M., Claustre H., Mignot A., et al. (2021). Deep chlorophyll maxima in the global ocean: Occurrences, drivers and characteristics. *Global Biogeochem. Cycles* **35**:e2020GB006759. DOI:10.1029/2020GB006759
14. Zakem E.J., Al-Haj A., Church M.J., et al. (2018). Ecological control of nitrite in the upper ocean. *Nat. Commun.* **9**:1206. DOI:10.1038/s41467-018-03553-w
15. Garcia N.S., Bonachela J.A. and Martiny A.C. (2016). Interactions between growth-dependent changes in cell size, nutrient supply and cellular elemental stoichiometry of marine *Synechococcus*. *ISME J.* **10**:2715–2724. DOI:10.1038/ismej.2016.50
16. Kana T.M. and Glibert P.M. (1987). Effect of irradiances up to 2000 μE m−2 s−1 on marine Synechococcus WH7803—I. *growth, pigmentation, and cell composition. Deep Sea Res. Part A Oceanogr. Res. Pap.* **34**:479–495. DOI:10.1016/0198-0149(87)90001-X
17. Liu H., Bidigare R., Laws E., et al. (1999). Cell cycle and physiological characteristics of Synechococcus (WH7803) in chemostat culture. *Mar. Ecol. Prog. Ser.* **189**:17–25. DOI:10.3354/meps189017
18. Six C., Thomas J., Brahamsha B., et al. (2004). Photophysiology of the marine cyanobacterium Synechococcus sp. WH8102, a new model organism. *Aquat. Microb. Ecol.* **35**: 17–29. DOI: 10.3354/ame035017
19. Baer S.E., Lomas M.W., Terpis K.X., et al. (2017). Stoichiometry of *Prochlorococcus, Synechococcus*, and small eukaryotic populations in the western North Atlantic Ocean. *Environ. Microbiol.* **19**:1568–1583. DOI:10.1111/1462-2920.13672
20. Dutkiewicz S., Hickman A.E., Jahn O., et al. (2015). Capturing optically important constituents and properties in a marine biogeochemical and ecosystem model. *Biogeosciences* **12**:4447–4481. DOI:10.5194/bg-12-4447-2015
21. Geider R., MacIntyre H. and Kana T. (1997). Dynamic model of phytoplankton growth and acclimation:responses of the balanced growth rate and the chlorophyll a:carbon ratio to light, nutrient-limitation and temperature. *Mar. Ecol. Prog. Ser.* **148**:187–200. DOI:10.3354/meps148187
22. Inomura K., Omta A.W., Talmy D., et al. (2020). A mechanistic model of macromolecular allocation, elemental stoichiometry, and growth rate in phytoplankton. *Front. Microbiol.* **11**:86. DOI:10.3389/fmicb.2020.00086
23. Inomura K., Deutsch C., Jahn O., et al. (2022). Global patterns in marine organic matter stoichiometry driven by phytoplankton ecophysiology. *Nat. Geosci.* **15**:1034–1040. DOI:10.1038/s41561-022-01066-2
24. Ward B.B. (1985). Light and substrate concentration relationships with marine ammonium assimilation and oxidation rates. *Mar. Chem.* **16**:301–316. DOI:10.1016/0304-4203(85)90052-0
25. Ward B.B. (2008). Chapter 5 - Nitrification in marine systems. Nitrogen in the marine environment (Elsevier), pp:199–261. DOI: 10.1016/B978-0-12-372522-6.00005-0
26. Olson R.J. (1981). 15N tracer studies of the primary nitrite maximum. *J. Mar. Res.* **39**:203–226. https://elischolar.library.yale.edu/journal_of_marine_research/1540/
27. Smith J.M., Chavez F.P. and Francis C.A. (2014). Ammonium uptake by phytoplankton regulates nitrification in the sunlit ocean. *PLoS ONE* **9**:e108173. DOI:10.1371/journal.pone.0108173
28. Armstrong R.A. (2006). Optimality-based modeling of nitrogen allocation and photoacclimation in photosynthesis. *Deep Sea Res. Part II Top. Stud. Oceanogr.* **53**:513–531. DOI:10.1016/j.dsr2.2006.01.020
29. Grosse J., Burson A., Stomp M., et al. (2017). From ecological stoichiometry to biochemical composition: Variation in N and P supply alters key biosynthetic rates in marine phytoplankton. *Front. Microbiol.* **8**:1299. DOI:10.3389/fmicb.2017.01299
30. Liefer J.D., Garg A., Fyfe M.H., et al. (2019). The macromolecular basis of phytoplankton C:N:P under nitrogen starvation. *Front. Microbiol.* **10**:763. DOI:10.3389/fmicb.2019.00763
31. Masuda Y., Yamanaka Y., Smith S.L., et al. (2021). Photoacclimation by phytoplankton determines the distribution of global subsurface chlorophyll maxima in the ocean. *Commun. Earth Environ.* **2**:128. DOI:10.1038/s43247-021-00201-y
32. McCarthy J.J. and Goldman J.C. (1979). Nitrogenous nutrition of marine phytoplankton in nutrient-depleted waters. *Science* **203**:670–672. DOI:10.1126/science.203.4381.670
33. Aksnes D.L., Ohman M.D. and Rivière P. (2007). Optical effect on the nitracline in a coastal upwelling area. *Limnol. Oceanogr.* **52**:1179–1187. DOI:10.4319/lo.2007.52.3.1179
34. Liefer J.D., White A.E., Finkel Z.V., et al. (2024). Latitudinal patterns in ocean C:N:P reflect phytoplankton acclimation and macromolecular composition. *Proc. Natl. Acad. Sci. USA* **121**:e2404460121. DOI:10.1073/pnas.2404460121

35. Gui J. and Sun J. (2024). Phytoplankton carbon to chlorophyll a model development: A review. *Front. Mar. Sci.* **11**:1466072. DOI:10.3389/fmars.2024.1466072
36. Smyth T., Moffat D., Tarran G., et al. (2023). Determining drivers of phytoplankton carbon to chlorophyll ratio at Atlantic Basin scale. *Front. Mar. Sci.* **10**:1191216. DOI:10.3389/fmars.2023.1191216
37. Lomas M.W., Baer S.E., Mouginot C., et al. (2021). Varying influence of phytoplankton biodiversity and stoichiometric plasticity on bulk particulate stoichiometry across ocean basins. *Commun. Earth Environ.* **2**:143. DOI:10.1038/s43247-021-00212-9
38. Yan X., Yang J.-Y.T., Xu M.N., et al. (2022). Isotope constraints on nitrogen dynamics in the upper water column of the South China Sea. *Front. Mar. Sci.* **9**:1104135. DOI:10.3389/fmars.2022.1104135
39. Yang J.T., Tang J., Kang S., et al. (2022). Comparison of nitrate isotopes between the South China Sea and western North Pacific ocean: Insights into biogeochemical signals and water exchange. *J. Geophys. Res. Oceans* **127**:e2021JC018304. DOI:10.1029/2021JC018304
40. Kessouri F., Ulses C., Estournel C., et al. (2017). Nitrogen and phosphorus budgets in the northwestern mediterranean deep convection region. *J. Geophys. Res. Oceans* **122**:9429–9454. DOI:10.1002/2016JC012665
41. Wirtz K. and Smith S.L. (2020). Vertical migration by bulk phytoplankton sustains biodiversity and nutrient input to the surface ocean. *Sci. Rep.* **10**:1142. DOI:10.1038/s41598-020-57890-2

FUNDING AND ACKNOWLEDGMENTS

This work was supported by a grant from the Simons Foundation (LS-ECIAMEE-00001549, Inomura). We greatly appreciate the discussion with Gabrielle Armin about the earlier version of cell flux model. The 1D physical model, phytoplankton growth and difference scheme of the simplified nitrogen ecosystem model (sNECO) were based on the study of Zakem et al.,[14] and we thank Emily J. Zakem for the permission to adapt the code from https://github.com/emilyzakem/eco-nitrify. The funders had no role in study design, data collection and analysis, decision to publish, or preparation of the manuscript.

AUTHOR CONTRIBUTIONS

M.D. and K.I. conceived the study and developed the model. M.D. performed the model simulation and analyzed the data. M.D. and J.C-C. visualized the results and prepared the figures. K.I. supervised this study, acquired funding and coordinated project administration. M.D. wrote the original draft, which was reviewed and edited by all the authors. All authors contributed to the manuscript and approved the final version.

DECLARATION OF INTERESTS

The authors declare no competing interests.

DATA AND CODE AVAILABILITY

The code of CFM-water column model and simplified nitrogen ecosystem model is available on GitHub: https://github.com/Snowoctopus/CFM-Nwatercolumn.git, https://github.com/Snowoctopus/simple_NECO.git.

SUPPLEMENTAL INFORMATION

It can be found online at https://doi.org/10.59717/j.xinn-geo.2026.100230.

LEAD CONTACT WEBSITE

Keisuke Inomura: https://www.inomura.com/